Biophysical Journal
Article

Biophysical Society

Crowding-induced phase separation and gelling by co-condensation of PEG in NPM1-rRNA condensates

Alain A. M. André,[1] N. Amy Yewdall,[1] and Evan Spruijt[1,*]
[1]Institute for Molecules and Materials, Radboud University, Heyendaalseweg 135, 6525 AJ Nijmegen, the Netherlands

ABSTRACT The crowdedness of the cell calls for adequate intracellular organization. Biomolecular condensates, formed by liquid-liquid phase separation of intrinsically disordered proteins and nucleic acids, are important organizers of cellular fluids. To underpin the molecular mechanisms of protein condensation, cell-free studies are often used where the role of crowding is not investigated in detail. Here, we investigate the effects of macromolecular crowding on the formation and material properties of a model heterotypic biomolecular condensate, consisting of nucleophosmin (NPM1) and ribosomal RNA (rRNA). We studied the effect of the macromolecular crowding agent poly(ethylene glycol) (PEG), which is often considered an inert crowding agent. We observed that PEG could induce both homotypic and heterotypic phase separation of NPM1 and NPM1-rRNA, respectively. Crowding increases the condensed concentration of NPM1 and decreases its equilibrium dilute phase concentration, although no significant change in the concentration of rRNA in the dilute phase was observed. Interestingly, the crowder itself is concentrated in the condensates, suggesting that co-condensation rather than excluded volume interactions underlie the enhanced phase separation by PEG. Fluorescence recovery after photobleaching measurements indicated that both NPM1 and rRNA become immobile at high PEG concentrations, indicative of a liquid-to-gel transition. Together, these results provide more insight into the role of synthetic crowding agents in phase separation and demonstrate that condensate properties determined in vitro depend strongly on the addition of crowding agents.

SIGNIFICANCE Within the crowded cellular interior, biomolecular condensates form via liquid-liquid phase separation of proteins and nucleic acids. The high intracellular concentrations of macromolecules is often approximated in vitro using, polymeric crowding agents, such as PEG. However, these crowding agents are commonly selected because of their commercial availability and water solubility; their influence on phase separation and the resulting physicochemical properties of condensates are seldom studied. Here, we use biophysical methods to show PEG induces phase separation of a model condensate through co-condensation, rather than volume exclusion. As a consequence, crowding changes the partitioning, concentrations, and viscoelastic properties of the condensates significantly, which puts studies aimed at quantifying the material properties of biomolecular condensates using in vitro models into new perspective.

INTRODUCTION

One of the most fascinating aspects of the inner biochemistry of a cell is how it functions in an extremely crowded environment. Typical estimates indicate that cellular biopolymers, including proteins and RNA, occupy 20 to 30 vol % of the cell, limiting intracellular diffusion and making the cell's interior a very crowded place (1–3). To enable effective biomolecular reactions, the cellular organization is of great importance (4,5). Traditionally, membrane-bound organelles have been extensively studied for their roles in organizing biochemical processes. This research has recently entered a new phase, as biomolecular condensates, also referred to as membraneless organelles, were found to be involved in the regulation of several biological processes, including transcription (6–8), cell signaling (9,10), and ribosome biogenesis (11–13).

Biomolecular condensates benefit from the absence of a physical membrane barrier, giving these condensates dynamic properties: they can fuse, ripen, and wet membranes or become engulfed by other condensates (14). This reflects

Submitted July 26, 2022, and accepted for publication November 30, 2022.
*Correspondence: e.spruijt@science.ru.nl
Editor: Roland Winter.
https://doi.org/10.1016/j.bpj.2022.12.001

the molecular nature of these condensates: they are typically enriched in proteins containing intrinsically disordered regions (IDRs) and nucleic acids (11,15). The IDRs are not only disordered, but they also contain certain repetitive motifs, for example in the form of weakly charged patches (16,17). Condensation is typically driven by liquid-liquid phase separation (LLPS) of these sticky moieties in the IDRs, but it is not limited to IDRs, as structural domains have been found to act as effective stickers as well (18–20). The balance between intermolecular association being not too strong to avoid turning the condensate into a gel, and not too weak to avoid dissolving it, makes most condensates highly responsive to changes in their environment, such as salinity and crowding, or subtle changes to the molecular constituents, such as enzymatic product formation or post-translational modifications (4,21).

Many of the molecular mechanisms underlying condensate formation and phase behavior have been unraveled through in vitro (here: cell-free) experiments (22–25). However, the cell-free environment in which proteins are studied is often far from realistic intracellular conditions. Factors that are typically regulated in what are considered to be "physiological" conditions include ionic strength, pH, and temperature (26). In contrast, the high degree of crowding in a living cell is not commonly taken into account in cell-free experiments despite the fact that many studies have shown that crowding can have a significant effect on protein stability, complexation, and reactivity (3,4,27,28). When crowding is taken into account, the crowded cellular milieu is often mimicked by the addition of water-soluble polymers such as poly(ethylene glycol) (PEG), Ficoll, and dextran (29–34). Although these polymers are highly water soluble, PEG and dextran can also undergo segregative phase separation, ending up in separate phases (35,36). This indicates that they have nonnegligible interactions with each other, and it suggests that these and other crowding agents could also interact with disordered and structured biomolecules and affect their phase behavior.

Indeed, it has been recognized that volume exclusion alone often cannot explain the changes to protein assembly caused by polymeric crowders (37). Several studies have found associative interactions between a polymeric crowding agent like PEG and proteins (38–40). These interactions have been found to alter protein folding (38) and crystallization (41). A recent study also showed that PEG interacts with disordered protein fused sarcoma (FUS), which is known to undergo LLPS (42). Therefore, a systematic study of the effect of crowding agents on commonly studied biomolecular condensates is of great relevance to understand the role of crowding in LLPS, and in particular their implications for the appropriateness of in vitro condensate model systems.

Crowding agents can affect biomolecular condensates in three ways. 1) They could promote (or in theory also suppress) phase separation by enhancing the weak intermolecular interactions through excluded volume effects or co-condensation, thereby shifting the binodal line to lower concentrations (43) as shown for NPM1-S6N (29), homotypic NPM1 (30), and FUS condensates (44). 2) Crowding agents can co-localize into the dense phase, as has been observed for dextran (45), PEG (42), and Ficoll (46). This may be caused by the distinct local chemical environment (for instance, nuage bodies are thought to have a more hydrophobic interior (22)), but the change in composition could also lead to a further change in the local environment. 3) Finally, the enhanced intermolecular interactions and altered composition could result in a change of the biophysical properties. For example, the condensed phase could become more viscous or switch to a solid-like state, such as previously observed for FUS (44) and NPM1 (29,30).

Here, we investigate the presence of these three effects in a well-studied condensate model of NPM1-rRNA using the most prevalent crowding agent found in studies of protein phase separation, PEG. We show that PEG induces both homotypic and heterotypic phase separation, and we quantified the changes in the dilute and condensed phase. We observed the strongest crowding effect for NPM1, although there was no significant effect on rRNA in the dilute phase. Through confocal microscopy, we were able to prove that PEG weakly partitions into the condensed phase, where it causes a different increase in the NPM1 and rRNA density, thereby altering the condensate composition. Finally, using fluorescence recovery after photobleaching (FRAP), we measured the viscoelastic properties of both NPM1 and rRNA, which showed a rapid decrease of the mobile fraction in the presence of PEG.

MATERIALS AND METHODS

Materials

Unless otherwise stated all chemicals were purchased from Sigma-Aldrich, but mPEG (10 kDa)-rhodamine (PSB-2263) was purchased from Creative PEGWorks. All aqueous solutions were prepared in Milli-Q water (18.2 MΩ·cm), except for the rRNA stock solution, which was dissolved in nuclease-free water (Invitrogen).

Protein expression and purification

E. coli BL21 (DE3) was transformed with pET28a(+)hNPM1 (47). Bacterial cell cultures were grown in Luria-Bertani medium (LB medium) supplemented with 50 μg L^{-1} kanamycin at 37°C till OD_{600} reached 0.6–0.8 before expression was induced with 1 mM IPTG. Protein expression was carried out overnight at 18°C, and the cells were pelleted through centrifugation. Pellets were either stored at −80°C or directly used for purification. For purification, pellets were thawed on ice and resuspended in lysis buffer (10 mM Tris-HCl, pH 7.5, 300 mM NaCl, 20 mM imidazole) supplemented with 5 mM β-mercaptoethanol, 1× protease inhibitor (Roche), and 10 mM PMSF. Cell suspensions were either lysed by sonication (Sanyo Soniprep 500) or French Press homogenizer (Homogenizing Systems). The lysate was cleared through centrifugation at 20,000 *g* at 4°C for 30 min in a Beckman JA25.50 rotor. The supernatant was loaded on an equilibrated 5 mL His-trap column (GE healthcare/Cytiva) at 4°C. The loaded column was

washed with 10 column volumes (CV) lysis buffer and eluted with 3 CV elution buffer (20 mM Tris-HCl, pH 7.5, 300 mM NaCl, 5 mM β-mercaptoethanol, 500 mM imidazole). Protein-containing fractions were dialyzed overnight against SEC buffer (10 mM Tris-HCl, pH 7.5, 300 mM NaCl, 1 mM DTT) and concentrated to <5 mL using Amicon Ultra spin concentrators (Millipore, MWCO: 10 kDa). The concentrated protein sample was loaded on a Superdex 200 16/600 (GE healthcare) size exclusion column connected to an AKTA Basic FPLC (GE Healthcare) in SEC buffer. Elution was carried out at room temperature at 1 mL/min and monitored at 205 nm, 254 nm, and 280 nm. Fractions of the main peak were pooled and concentrated using Amicon-Ultra spin concentrators (Millipore, MWCO: 10 kDa). The concentration was determined using the NanoDrop One^{C} (Thermo Scientific), and aliquots were snap frozen in liquid nitrogen and stored at −80°C.

NPM1-Alexa488 labeling

NPM1-wt was labeled using AlexaFluor488 C5 maleimide dye (Thermo Fisher) according to manufacturer's protocol. In short, 100 μM NPM1 was dialyzed against 10 mM Tris-HCl (pH 7.5), 300 mM NaCl, and 1 mM TCEP. Using Amicon Ultra spin concentrator (Millipore MWCO: 10 kDa), the excess TCEP was removed, and 200 μM AlexaFluor488 C5 maleimide dye was added and incubated overnight at 4°C. Excess dye was removed through dialysis (Millipore, MWCO 3.5 kDa) against SEC buffer, and the concentration was determined using the NanoDrop One^{C}.

Ribosomal RNA isolation

E. coli BL21 (DE3) pLysS cells were grown at 37°C in LB medium till OD_{600} reached 1.2, and the cells were pelleted through centrifugation (5000 *g* at 4°C for 15 minutes). Pellets were washed twice in S30 buffer A (50 mM Tris-HCl, pH 7.7, 60 mM potassium glutamate, 14 mM magnesium glutamate, 2 mM DTT), and resuspended in S30 buffer A (1 mL buffer to 1 gram cell pellet). This cell suspension was then homogenized through sonication (Sanyo Soniprep 150) and cleared through centrifugation (15,000 rpm at 4°C for 25 min) in a Beckman JA25.50 rotor. Ribosomes were isolated by ultracentrifugation for 3 h at 50,000 rpm (Beckman-Coulter Optima-90, with a fixed angle 90-Ti rotor). The glassy rough ribosome pellets were dissolved overnight in S30 buffer B (5 mM Tris-HCl, pH 8.2, 60 mM potassium glutamate, 14 mM magnesium glutamate, 2 mM DTT) at 4°C. The ribosomal RNA (rRNA) was isolated from the ribosomes through standard phenol chloroform extraction using phenol:chloroform:isoamyl alcohol (PCI, 49.5:49.5:1). The final rRNA concentration was determined using the NanoDrop One^{C}, where 1 $OD_{600} = 40\ \mu g\ mL^{-1}$ RNA, and stored at −80°C.

RNA-Alexa647 labeling

The 3′ hydroxyl-end of the rRNA was labeled with AlexaFluor647 hydrazide using a periodate oxidation reaction (47–49). In short, to 80 μL of rRNA (3.4 mg mL^{-1}), 7 μL of nuclease-free water, 3.33 μL of 3 M sodium acetate (pH 5.2), and 10 μL of 25 mM sodium periodate (freshly prepared in water on the day) was added. The mixture was incubated on ice for 50 min. Subsequently, 20 μL of 3 M sodium acetate (pH 5.2) and 80 μL nuclease-free water was added. The activated RNA was then precipitated by addition of 400 μL isopropanol through cooling it on ice for at least 1 h. The RNA was then spun down (14,000 *g* at 4°C for 15 min). The supernatant was removed, and 150 μL of ice-cold ethanol was added to the pellet without mixing. After another centrifugation step, and removal of the supernatant, the RNA was mixed into the reaction buffer (100 mM sodium acetate, pH 5.2, 25 nmol AlexaFluor647 hydrazide). The reaction was left over 48 h, after which the labeled RNA was isolated through an isopropanol and ethanol precipitation. The rRNA-A647 was then redissolved in 80 μL of nuclease-free water. The concentration was determined using the NanoDrop One^{C}.

Preparation of NPM1-rRNA condensates

NPM1-AlexaFluor488 (NPM1-A488) stock solutions were prepared at 200 μM with 1:9 molar ratio AlexaFluor488 labeled NPM1 to unlabeled NPM1 in 10 mM Tris-HCl (pH 7.5) and 300 mM NaCl. NPM1-A488 aliquots of 20 μL were snap frozen and stored at −80°C.

A 35 wt % PEG-rhodamine stock solution was prepared by mixing 347 mg/mL PEG (average molecular weight of 10 kDa) with 3 mg/mL mPEG-5,6-corboxytetramethylrhodamine (average molecular weight of 10 kDa). The stock solution was aliquoted in small portions and stored at −20°C.

The order of components for a typical experiment consists of first mixing the PEG (from a 35 wt % stock described above), with the buffer (from a 4× stock of 40 mM Tris-HCl (pH 7.5), 600 mM NaCl) and then diluted to the required final volume, often 30 μL at room temperature. 15 min before measuring the NPM1-A488 and rRNA were added to the premixed diluted buffer.

Preparation of modified glass coverslips

Ibidi 18-well chambered slides (#1.5) were first cleaned using oxygen plasma and directly afterward incubated in a 0.01 mg/mL solution of PLL(20)-g[3,5]-PEG(2) (SuSoS AG, Switzerland) in 10 mM HEPES buffer (pH 7.4) for at least 1 h at room temperature. Ibidi chambers were rinsed several times with Milli-Q water and dried with pressurized air. Modified glass slides were stored at −20°C.

Quantification of the dilute phase

A typical sample of 30 μL was prepared in 10 mM Tris (pH 7.5) and 150 mM NaCl with varying concentrations of PEG, NPM1/NPM1-A488 (1:9 molar ratio labeled), and rRNA-A647 (only labeled) as described above. After incubating for 15–20 min at room temperature, the condensed phase was separated from the dilute phase by centrifugation at 21,000 *g* for 20 min at room temperature. The dilute phase was then transferred to a 384-well plate (Nunc, flat bottom), and the fluorescence intensity was measured on a plate reader (Tecan Spark M10) at 485/535 nm for NPM1-A488 and 620/680 nm for rRNA-A647. Concentrations of the dilute phase were calculated based on calibration curves (Fig. S1).

Quantification of the condensed phase by confocal microscopy

The tiny, combined volume of the condensate droplets (<0.1 μL) made an equivalent analysis of the absolute concentrations by fluorescence spectroscopy impossible. Therefore, we analyzed fluorescence intensities inside the condensates by confocal microscopy, which allows comparing the composition of the condensates at different PEG concentrations and the degree of condensation relative to the dilute phase (via partition coefficients). Images for partitioning were acquired on a Leica Sp8x confocal inverted microscope (Leica Microsystems, Germany) equipped with a DMi8 CS motorized stage, a pulsed white light laser, and 2 × HyD SP GaAsP and 2× PMT detectors. Images were recorded using the LAS X v.3.5 acquisition software, using an HC PL APO 100×/1.40 oil immersion objective. For the NPM1, the laser was set to 495 nm, and a HyD detector was used, measuring at 505–550 nm. For the rRNA, the laser was set to 653 nm, and a HyD detector was used, measuring 663–778 nm. For the PEG, the laser was set to 573 nm, and a PMT detector was used, measuring 583–649 nm with a gain of 800 V.

Samples were prepared as described above. After incubation of NPM1-rRNA condensates for 15 min, the sample was transferred to the modified Ibidi-18 well chambers, and the condensates were allowed to settle to the bottom of the chamber for 10 min. Partitioning coefficients were analyzed by MATLAB, and the background was subtracted by measuring nonfluorescent condensates at the same settings as for the fluorescent images. The partitioning coefficient was then calculated using the following: $K_p = (I_{condensate} - I_{background})/(I_{dilute} - I_{background})$, where $I_{condensate}$ is the average intensity of all condensates in one frame, and I_{dilute} the average intensity of the area without condensates. Standard deviations were determined of at least three sets of K_p values derived from three different images.

FRAP analysis

For FRAP analysis, time-lapse videos were recorded at room temperature on a CSU X-1 Yokogawa spinning disk confocal unit connected an Olympus IX81 inverted microscope, using an ×100 piezo-driven oil immersion objective (NA 1.3) and 488-, 561-, or 640-nm laser beams. Emission was measured with a 200-ms exposure time at a rate of 120 frames per minute, using an Andor iXon3 EM-CCD camera. The acquired images have a pixel size of 141 nm and a field of 72 x 72 μm^2. For bleaching, a small region of interest was selected in the middle of a condensed droplet. The 488- or 640-nm laser line was set to 100% laser power using 75 pulses of 200 µs. The recovery was then imaged at reduced laser intensity with a time interval of 500 ms.

Recovery profiles were analyzed using ImageJ, and the normalized intensities were fitted to a 2D-diffusion with a fixed boundary (50). We used the resulting exponential decay equation $I_{normalized} = A(1\text{-}e^{-bt})+C$, from which we obtained the parameters A, b, and C. The recovery half-life was then determined at $t_{1/2} = ln(2)/b$.

RESULTS AND DISCUSSION

PEG shifts the phase diagram boundary of NPM1-rRNA

Inspired by the numerous membraneless organelles that contain both proteins and RNA, we chose a heterotypic system consisting of a 34.7 kDa protein called nucleophosmin-1 (NPM1), which assembles into pentamers through its N-terminal oligomerization domain (OD), and ribosomal RNA (rRNA) as model condensate. This system is illustrated in Fig. 1 *A*, and it forms liquid droplets under "physiological" conditions (here defined as physiological salt by 10 mM Tris, 150 mM NaCl), even without crowding. By labeling both NPM1 and rRNA with fluorophores, we could observe that indeed the rRNA co-localizes into the dense NPM1 droplets (Fig. 1 *B*), in agreement with our previous study (47). We found a maximum degree of phase separation, as inferred from microscopy analysis, at a NPM1:rRNA ratio of 20 µM NPM1 : 150 ng μL^{-1} (440 µM nucleotides) rRNA (19,47). This corresponds roughly to one pentamer NPM1 interacting with 110 nucleotides of rRNA. When keeping this ratio constant, we could decrease the protein concentration to a lower limit of 10 µM and still observe liquid condensates (Figs. 1 *C* and S2).

When we added PEG (10 kDa), a commonly used crowding agent, to the mixtures of NPM1 and rRNA, we observed phase separation at lower NPM1 concentrations. For 2 wt % PEG, we could observe phase separation for concentrations down to 2.5 µM NPM1 and 19 ng μL^{-1} (56 µM nucleotides) rRNA (Figs. 1 *C*, S2, and S3), which suggests that PEG enhances the association between protein and RNA. Moreover, we found that at 2 wt % PEG, NPM1 could also phase separate without RNA at 10 µM NPM1 and higher into apparently homotypic droplets (Fig. 1 *C* and S4). These findings are in agreement with a previous study of Kriwacki and co-workers, who showed that no second component, such as arginine-rich peptides or rRNA, is needed for phase separation of NPM1 under PEG-based crowding conditions (29,30). These findings suggest that crowding by PEG not only enhances associative interactions between NPM1 and rRNA, but it enhances the self-interactions of NPM1 even more. Assuming that volume exclusion by the crowding agents is responsible for enhancing the intermolecular interactions, the observed effects could be explained by the structural differences between NPM1 and rRNA: the protein NPM1 has a more globular shape and a larger effective radius than the tube radius of polymeric rRNA and may therefore experience stronger volume exclusion due to crowders. Crowding by PEG will thus likely affect the concentrations of NPM1 and rRNA in both the dilute and the dense (condensate) phase in a nontrivial way. Therefore, we next sought to quantify the NPM1-rRNA phase boundary and condensate composition under crowding conditions.

PEG reduces only NPM1 concentrations in the dilute phase

As introduced above, excluded volume theory predicts that crowding enhances the effective attractions between macromolecules by increasing the entropy of the crowders upon complexation of the macromolecules. For our phase separating system, enhanced attraction could result in phase separation at lower concentrations, as suggested by the measurements in Fig. 1 *C*. To obtain a quantitative understanding of the effect of crowding on phase separation between NPM1 and rRNA, and how this affects their concentrations in the dilute and condensed phase, we determined the compositions of the droplets and supernatant as function of the amount of crowding agent PEG.

First, we examined the concentrations of NPM1 and rRNA in the dilute phase. The condensates were separated from the dilute phase by centrifugation (Fig. S5). We quantified the concentration of NPM1 and rRNA in the dilute phase for three different overall mixing ratios. In all cases, the addition of PEG reduced the concentration of NPM1 in the dilute phase, whereas the rRNA remained approximately constant or even increased (Fig. 2 *A*). It is clear that this is not the expected behavior for a classical crowding agent that enhances the attraction between NPM1 and rRNA. In that case, the saturation concentration of both NPM1 and rRNA should decrease with increased crowding, although the relative degree of decrease might depend on the

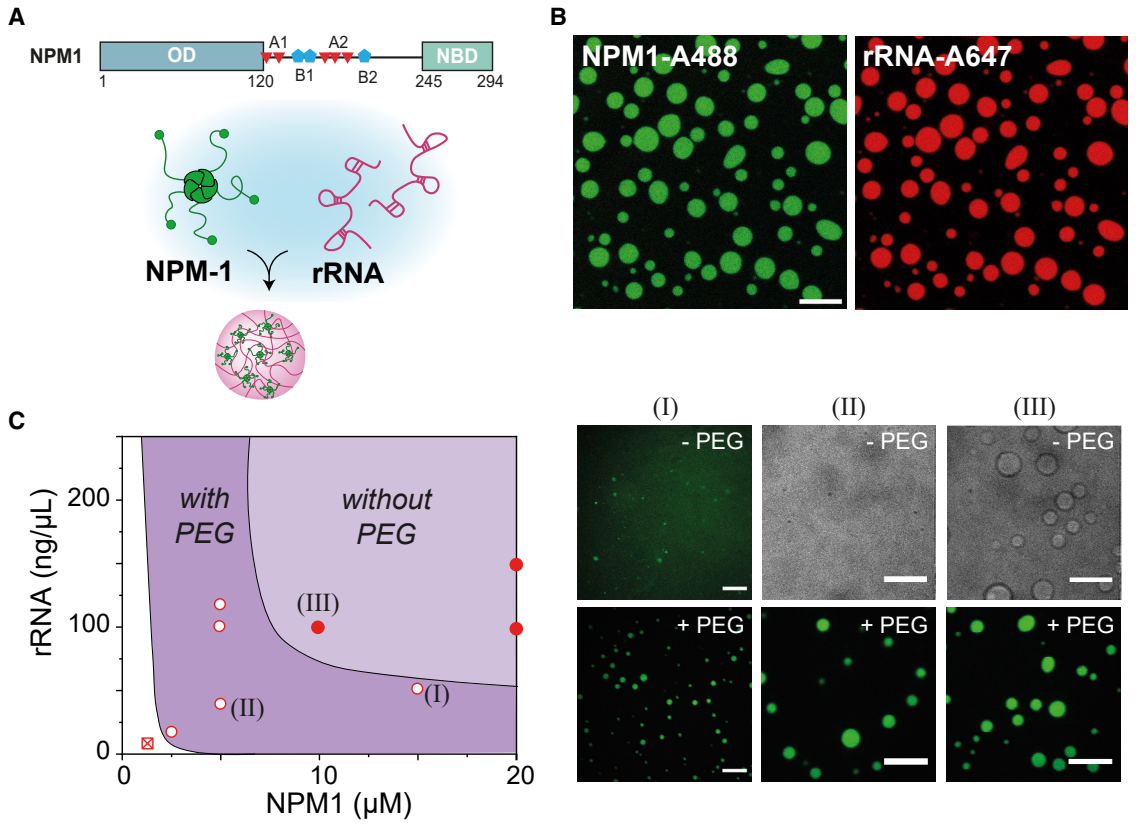

FIGURE 1 PEG-induced phase separation of NPM1-rRNA. (*A*) Schematic illustration of nucleophosmin (NPM1) protein domains and the formation of condensates with rRNA. NPM1 encodes for a structural N-terminal oligomerization domain (OD) and a C-terminal nuclear binding domain (NBD) linked by an intrinsically disordered region with two acidic tracts (A1 and A2) and two weak basic tracts (B2 and B2). Pentamers of NPM1 phase separate with rRNA into condensates in vitro. (*B*) Fluorescent microscopy images of NPM1-rRNA condensates at 10 μM NPM1-Alexa488; 150 ng μL^{-1} rRNA-Alexa647 (in 10 mM Tris, pH 7.5, 150 mM NaCl). Scale bar, 10 μm. (*C*) Schematic representation of the shift in phase boundary of NPM1-rRNA liquid-liquid phase separation as determined by preparing mixtures with different overall composition (51). Note that the drawn lines indicating the phase boundaries without PEG and with 2 wt % PEG are drawn to guide the eye and do not represent accurate binodal lines, in particular at rRNA concentrations above 125 ng μL^{-1}. Three conditions have been highlighted with roman numerals, and microscopic images in the presence or absence of 2 wt % PEG are shown to the right: (I) 15 μM NPM1, 50 ng μL^{-1} (147 μM nt) rRNA, (II) 5 μM NPM1, 37.5 ng μL^{-1} (110 μM nt) rRNA, (III) 10 μM NPM1, 75 ng μL^{-1} (220 μM nt) rRNA. Scale bars, 10 μm.

overall mixing ratio. Instead, we found that the rRNA saturation concentration remained constant for all mixing ratios. Crowding thus seems to leave the interaction between NPM1 and rRNA unchanged, although it enhances the interactions of NPM1 with itself, as the saturation concentration of NPM1 decreased significantly. Our results regarding the NPM1 concentrations in the dilute phase corroborate what has previously been observed for homotypic NPM1 condensation (29): crowding decreased the solubility of NPM1. However, it was also observed that the ratio between the arginine-rich SURF6 peptide (S6N) and NPM1 remained constant with increasing crowding concentrations, probably because the short peptide partitions as a client into the homotypic NPM1 droplets.

To analyze the effect of PEG in more detail, we focused on one ratio of NPM1:rRNA (10 μM NPM1 with 100 ng μL^{-1} (293 μM nt) rRNA), and looked at several concentrations of PEG (Fig. 2 *B* and *C*). The dilute phase NPM1 concentration gradually decreased from 7.5 μM without crowding to 2.5 μM NPM1 at 10 wt % PEG (Fig. 2 *B*). We did not observe a plateau at high crowding, despite the fact that the condensates had turned into gel-like structures with very little relaxation already at 2 wt % PEG (see also crowding reduces condensate fluidity section), but rather a gradual decrease that becomes asymptotic toward zero, in agreement with simple theoretical predictions for crowding-induced phase separation. For rRNA, we observed no clear change in the concentration in the dilute phase, as was found for other mixing ratios as well: it remained constant around 100 ng μL^{-1} (Fig. 2 *C*).

PEG partitions into condensates and increases local concentrations of all components

We next analyzed how crowding affects the composition of condensates by studying the condensed phase in more detail. We analyzed the relative changes in the composition of the condensates using fluorescence microscopy (Fig. 3 *A*

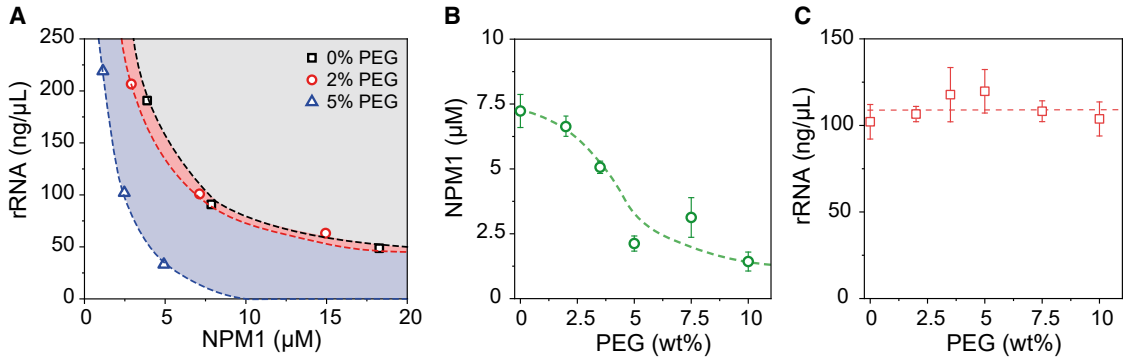

FIGURE 2 PEG reduces NPM1 concentration and not the rRNA concentrations in the dilute phase. (*A*) Concentrations of NPM1 plotted against rRNA in the dilute phase for three fixed NPM1:rRNA ratios: 5:150, 10:100, and 20:50 (μM NPM1:ng μL^{-1} rRNA) at three different PEG concentrations. A mass concentration of 150 ng μL^{-1} rRNA corresponds to 440 μM nt. (*B* and *C*) Addition of PEG to 10 μM NPM1 and 100 ng μL^{-1} rRNA reduces the concentration of NPM1 in the dilute phase (*B*) but not for rRNA (*C*). The error bars in these figures represent standard deviations from triplicate measurements, and the dashed lines are present to guide the eye. To see this figure in color, go online.

and *D*). To avoid interference from fluorophore self-quenching or homo-FRET, we took care to use labeled NPM1 and rRNA at low enough concentrations that the fluorophores are further apart than their typical homo-FRET distance (52). From the microscopy images of condensates, we analyzed both the absolute fluorescence intensity in the condensates and the intensity relative to surrounding dilute phase (hereafter: the partitioning coefficient (K_p)). The fluorescence intensity can be used to directly compare the relative amounts of NPM1 and rRNA in the condensates, whereas the partitioning can be used to compare the extent to which the condensed and dilute phase concentrations become more separated from each other (the degree of condensation relative to the dilute phase). Both the fluorescence intensity and partitioning are independent of the condensate size.

Confocal microscopy images revealed a threefold increase in fluorescence intensity of NPM1 from 13 to 39 upon addition of 2 wt % PEG (Fig. 3 *B*). The partitioning coefficient (K_p) for NPM1 (Fig. 3 *C*) showed a similar increase between 0 and 2 wt % PEG, as the NPM1 concentration in the dilute phase decreased only slightly. Further increasing the overall concentration of PEG did not lead to additional increase in NPM1 fluorescence within the dense phase, suggesting NPM1 concentrations within the condensate increased and plateaued after PEG addition. The partitioning coefficient increased because the NPM1 concentration in the dilute phase kept decreasing (Fig. 2 *B*). This increase in NPM1 concentration is expected if the PEG crowders enhance the association between NPM1 proteins, although the magnitude of the observed increase is higher than expected for a crowder at approximately 5 vol % (53). However, the observed plateau in NPM1 concentration is not consistent with PEG having only excluded volume interactions. Indeed, for purely excluded volume interactions between crowder and the phase-separating biomolecules, we would expect the local concentration of biomolecules inside the condensates, and thereby their density, to continue increasing with increased crowder concentration. This would translate into a higher binodal condensate concentration. Our results suggest that the interactions between NPM1 and PEG may not be limited to volume exclusion.

In contrast to NPM1, rRNA showed a much lower partitioning into the condensates ($K_p = 5$) in the absence of PEG, and the rRNA concentration increased only slightly upon addition of PEG (Fig. 3 *B*). At PEG concentrations from 0 to 2 wt %, the rRNA intensity in the dense phase increased about 25%, from 11 to 13.5 (Fig. 3 *B*), whereas the local NPM1 intensity increased threefold. This suggests that PEG changes the relative amounts of NPM1 and rRNA inside the condensates, possibly because it enhances the self-interaction between NPM1 proteins. Upon further increasing the PEG concentration to 7.5 wt %, the rRNA intensity (and partitioning) increased significantly, ultimately reaching a similar threefold increase as NPM1 (Fig. 3 *B* and *C*). PEG is known to enhance folding of RNA into more compact states (54,55), which could explain the higher concentration of rRNA inside the condensates. The strongly increased concentrations of both NPM1 and rRNA at the highest PEG concentration may suggest that the condensates are no longer simple liquids, but that they are kinetically trapped in a gel state, as we will discuss further below.

Finally, we also looked at the distribution of the crowding agent PEG over the two phases (Fig. 3). If the first-order liquid-liquid phase transition is enhanced by excluded volume interactions of the crowder with the proteins and RNA, and the contribution of the crowders to the osmotic pressure is ignored, then the concentration of crowders should be the same in the dilute and condensed phase. In reality, the high local concentration of biomolecules in the condensates excludes volume for the crowder molecules, and therefore, we expect that crowders are weakly depleted from the condensates. However, when we measured the distribution of PEG over both phases via fluorescence microscopy, we found that PEG was enriched in the condensed

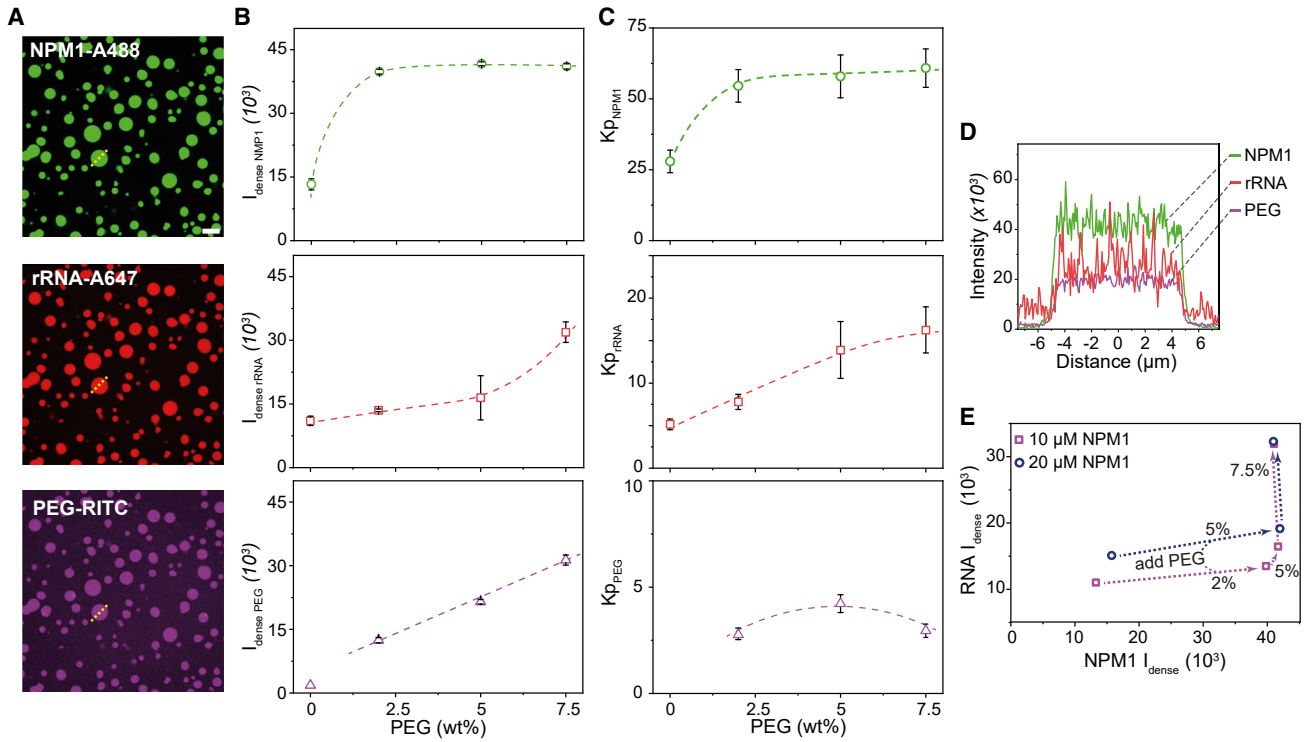

FIGURE 3 Confocal microscopy analysis of NPM1-rRNA condensates under crowded conditions. (*A*) Fluorescence images of NPM1-Alexa488, rRNA-Alexa647, and PEG-rhodamine, indicating PEG co-localizes into the condensed phase (20 μM NPM1, 150 ng μL^{-1} rRNA, 5 wt % PEG). Scale bar, 10 μm. (*B* and *C*) Average fluorescence intensities (*B*) and partitioning coefficients (K_p) (*C*) of NPM1, rRNA, and PEG plotted against the concentrations of PEG. (*D*) Intensities profile across one single condensate (*dashed line in A*). (*E*) Graph representing the influence of crowding on the intensities (and therefore concentration) of NPM1 and rRNA within condensates. The errors in this figure are standard deviations from triplicate measurements, and all dotted lines and arrows are to guide the eye. To see this figure in color, go online.

phase by a factor of 3 (Fig. 3 *B* and *C*). To minimize the effect of the dye, less than 0.1% of the PEG was labeled in this study. Interestingly, the enrichment was independent of crowding concentration, and it suggests that PEG exhibits associative interactions with NPM1 or rRNA or both. Therefore, the classical picture of PEG as an inert crowding agent that interacts via excluded volume interactions with biomolecules is not accurate. Instead, PEG seems to co-condense with NPM1 and/or rRNA in a form of ternary associative phase separation.

Partitioning of crowding agents into condensates is system dependent. Similar to our observations with PEG, the small molecular weight dextran (4.4 kDa) crowder was reported to partition into LAF1 RGG protein (45). In another study, the authors observed a weak exclusion of PEG (8 kDa), and enrichment of Ficoll (70 kDa) in coacervates made of spermine and polyuridylic acid (polyU) (46). Both types of crowders were hypothesized to enhance the favorable base stacking of polyU. Indeed, their results suggest that, for spermine-polyU coacervates, PEG behaves more like an inert crowder that does not specifically interact with the RNA in the dense phase. From this, we can infer that in our system of NPM1-rRNA, PEG is mostly associated with the NPM1 protein, in agreement with our observations of the decrease in NPM1 concentration in the dilute phase as the PEG concentration was increased (Fig. 2 *B*). This suggests that PEG-induced phase separation of homotypic NPM1 droplets is likely driven by a co-condensation of PEG and NPM1 (Fig. S4). The same may be the case for a significant number of other homo- and heterotypic IDP-based condensates that have been reported in the presence of PEG (4); for example, recently PEG was reported to interact with FUS-protein condensates (42).

Finally, our results show PEG co-condensation can alter condensate composition, by changing component ratios of NPM1 and rRNA. This is in contrast to NPM1-S6N condensates where component ratios were maintained in a 4:1 ratio with increased crowding, as the interactions in this system are electrostatic (29). Weak associations between the PEG and NPM1 underlie PEG co-condensation, which also increased the overall macromolecular concentration within the condensed phase. By extension, a similar mechanism may play a role in the crowded environment in the cell: besides excluded volume interactions, there may be many (weak) soft repulsive or attractive forces (3,56) between all the crowders and phase-separating IDRs, which could result in promotion of phase separation through co-condensation or segregation (57). A recent study from the Rosen

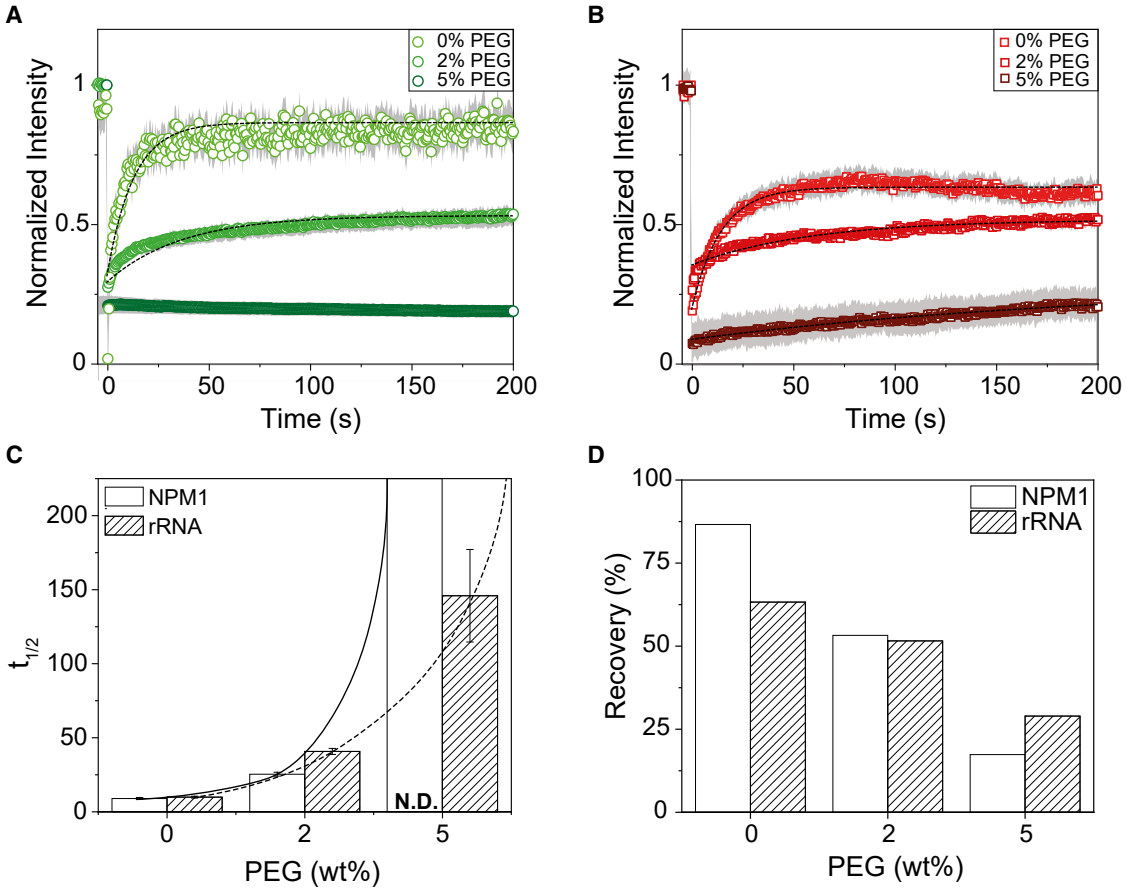

FIGURE 4 PEG changes the viscoelastic properties of NPM1 and rRNA. (*A* and *B*) The average FRAP recovery curves of NPM1 (*A*) and rRNA (*B*) upon increasing PEG crowding from three bleached droplets. The gray areas are standard deviations calculated from three independent measurements. The lines represent model fits from which the $t_{1/2}$ and total recovery were determined. The recovery of NPM1 at 2% PEG was better fitted with model containing two populations (Fig. S6). (*C*) Calculated half-time ($t_{1/2}$) of NPM1 and rRNA at different concentrations of PEG. The lines are there to guide the eye, and the error bars represent standard deviations from triplicate measurements. (*D*) Mobile fraction from the total recovery determined from the FRAP curves. To see this figure in color, go online.

lab showed that the material properties of yeast P-bodies are strongly dependent on the composition (58). This might indicate that the material properties of our NPM1-rRNA condensates formed in the presence of crowding agents are altered, as we investigated next.

Crowding reduces condensate fluidity

LLPS is characterized by the formation of droplets that typically exhibit rapid recovery of FRAP. Indeed, our model system shows full and fast recovery after photobleaching in the absence of PEG (Fig. 4). The mobile fraction correlates to the recovery percentage, and for NPM1 in buffer, this is almost 90%, and for rRNA around 65% (Fig. 4 *D*). This indicates that NPM1 shows almost a full recovery, since the total recovery was not corrected for the size of bleached area. From the recovery curves, we were able to determine the recovery half-time ($t_{1/2}$), which was for both NPM1 and rRNA approximately 10 s. Thus, although NPM1 and rRNA have similar characteristic recovery times, a larger fraction of the rRNA in condensates was immobile compared with NPM1. We attribute this to possible RNA-RNA interactions (47).

The addition of PEG reduced the mobile fraction of both NPM1 and rRNA in the condensed phase significantly: 2% PEG decreased the mobile fraction of both NPM1 and rRNA to 50%, whereas the recovery half-time increased to 25 s and 40 s, respectively. Interestingly, the recovery curves of NPM1 at 2% PEG suggest that there are two populations of NPM1 (Fig. S6 *D*): the fast-moving population has a similar half-time as NPM1 at 0% PEG, and the slow-moving population, which we could tentatively interpret as NPM1 clusters, is significantly slower ($t_{1/2}$ = 71 s). When we increased the PEG concentration further to 5%, both NPM1 and rRNA became completely immobile, indicating that the condensates are no longer liquid droplets governed by LLPS, but they have turned into gels.

The solidifying effect of PEG on both NPM1 and rRNA is interesting compared with our previous results. For instance, our lab showed that physiological concentrations of Mg^{2+}

were only affecting the rRNA diffusion in NPM1-rRNA condensates (47) by enhancing interactions between the rRNA molecules. Kriwacki and co-workers demonstrated that the addition of the arginine-rich domain SURF6 could liquefy homotypic NPM1 condensates (29). These newly formed NPM1-SURF6 condensates depend on oppositely electrostatic interactions, whereas NPM1-rRNA condensation is considered to rely on the RNA recognition motifs (RRMs) present in NPM1.

Taking into account that PEG is present within the condensed phase (Fig. 3), we hypothesize that co-condensation of PEG is solidifying NPM1-rRNA droplets in vitro. Since PEG is not fulfilling the classical crowding model of an inert macromolecule, we observe that PEG likely binds to NPM1 without affecting the ability of NPM1 to bind rRNA via the RRMs. The co-condensation of PEG and NPM1 strongly increases the NPM1 content, but it also reduces their diffusion. The rRNA remains condensed with the NPM1 via binding to the RRMs, but its concentration is not increased as much as NPM1 due to weakly unfavorable interactions with the PEG, as also suggested by the work of Keating and co-workers (46). Nevertheless, the higher local concentration of NPM1 also decreases the diffusivity of rRNA, as it is more likely to be bound by multiple RRMs of NPM1. Above a threshold PEG concentration, the local interactions between NPM1-NPM1 and NPM1-PEG become too strong, and their mobility decreases sharply, which is reflected by the absence of NPM1 recovery in Fig. 4 *C*.

CONCLUSIONS

In conclusion, we reported that the crowding agent PEG could induce and enhance phase separation of a model biomolecular condensate consisting of NPM1-rRNA. By quantifying the compositions of both the condensed and dilute phase, we could deduce that only the protein component NPM1 is depleted from the dilute phase and enriched in the condensed phase. Although the concentration of rRNA remained constant in the dilute phase, the condensed phase showed a slight PEG-dependent enrichment, possibly due to a more condensed state of the dense phase. Through fluorescent labeling of the crowding agent, we found that, surprisingly, PEG is also enriched in the condensed phase, suggesting that it enhances phase separation by co-condensing with NPM1 rather than through excluded volume interactions. These results also indicate that partitioning of "crowding agents" can change condensate compositions and material properties, and that even crowders that are widely believed to be inert can have significant interactions with biomolecules that undergo LLPS. This is relevant to the crowded environment of the cell as well: it is very likely that an important fraction of the macromolecules present in the cell exhibit weak repulsive or attractive interactions with the components of membraneless organelles, which results in altered composition and material properties compared with their in vitro reconstituted analogs. Finally, our results also put in vitro condensates formed in the presence of common crowding agents in a new perspective and suggest that addition of common crowding agents could affect in vitro phase separation systems and therefore should be selected with care.

SUPPORTING MATERIAL

Supporting Material can be found online at https://doi.org/10.1016/j.bpj.2022.12.001.

AUTHOR CONTRIBUTIONS

A.A.M.A.: conceptualization, methodology, investigation, analysis, and writing. N.A.Y.: methodology of rRNA labeling and writing. E.S.: conceptualization, software, writing, supervision, and funding acquisition.

ACKNOWLEDGMENTS

The authors thank Prof. Richard Kriwacki (St. Jude Children's Research Hospital) for providing us with the NPM1-GFP plasmid, Aafke Jonker and Frank Nelissen (Radboud University) for providing protocols to isolate ribosomes and labeling RNA, Merlijn van Haren (Radboud University) for providing a MATLAB script to determine partitioning coefficients and assisting with the FRAP analysis of the microscopy data, and Dr. Ioannis Alexopoulos (Radboud University, now Justus Liebig University) for his guidance in confocal microscopy. We would like to thank Prof. Wilhelm Huck (Radboud University) and Prof. Allen Minton (NIH) for fruitful discussions. This work was financially supported by the Netherlands Organisation for Scientific Research (NWO).

DECLARATION OF INTERESTS

The authors declare no competing interest.

REFERENCES

1. Fulton, A. B. 1982. How crowded is the cytoplasm? *Cell.* 30:345–347. https://doi.org/10.1016/0092-8674(82)90231-8.
2. Zimmerman, S. B., and S. O. Trach. 1991. Estimation of macromolecule concentrations and excluded volume effects for the cytoplasm of Escherichia coli. *J. Mol. Biol.* 222:599–620. https://doi.org/10.1016/0022-2836(91)90499-v.
3. Rivas, G., and A. P. Minton. 2016. Macromolecular crowding in vitro, in vivo, and in between. *Trends Biochem. Sci.* 41:970–981. https://doi.org/10.1016/j.tibs.2016.08.013.
4. André, A. A. M., and E. Spruijt. 2020. Liquid-liquid phase separation in crowded environments. *Int. J. Mol. Sci.* 21:5908. https://doi.org/10.3390/ijms21165908.
5. Shin, Y., and C. P. Brangwynne. 2017. Liquid phase condensation in cell physiology and disease. *Science.* 357:eaaf4382. https://doi.org/10.1126/science.aaf4382.
6. Guo, Y. E., J. C. Manteiga, J. E. Henninger, B. R. Sabari, A. Dall'Agnese, N. M. Hannett, J.-H. Spille, L. K. Afeyan, A. V. Zamudio, K. Shrinivas, B. J. Abraham, A. Boija, T.-M. Decker, J. K. Rimel, C. B. Fant, T. I. Lee, I. I. Cisse, P. A. Sharp, D. J. Taatjes, and R. A. Young. 2019. Pol II phosphorylation regulates a switch between transcriptional

and splicing condensates. *Nature.* 572:543–548. https://doi.org/10.1038/s41586-019-1464-0.

7. Ladouceur, A. M., B. S. Parmar, S. Biedzinski, J. Wall, S. G. Tope, D. Cohn…, 2020. Clusters of bacterial RNA polymerase are biomolecular condensates that assemble through liquid-liquid phase separation. *Proc. Natl. Acad. Sci. USA.* 117:18540–18549. https://doi.org/10.1073/pnas.2005019117.
8. Yamazaki, T., S. Souquere, T. Chujo, S. Kobelke, Y. S. Chong, A. H. Fox…, 2018. Functional domains of NEAT1 architectural lncRNA induce paraspeckle assembly through phase separation. *Mol. Cell.* 70:1038–1053.e7. https://doi.org/10.1016/j.molcel.2018.05.019.
9. Li, P., S. Banjade, H. C. Cheng, S. Kim, B. Chen, L. Guo…, 2012. Phase transitions in the assembly of multivalent signalling proteins. *Nature.* 483:336–340. https://doi.org/10.1038/nature10879.
10. Banjade, S., Q. Wu, A. Mittal, W. B. Peeples, R. V. Pappu, and M. K. Rosen. 2015. Conserved interdomain linker promotes phase separation of the multivalent adaptor protein Nck. *Proc. Natl. Acad. Sci. USA.* 112:E6426–E6435. https://doi.org/10.1073/pnas.1508778112.
11. Banani, S. F., H. O. Lee, A. A. Hyman, and M. K. Rosen. 2017. Biomolecular condensates: organizers of cellular biochemistry. *Nat. Rev. Mol. Cell Biol.* 18:285–298. https://doi.org/10.1038/nrm.2017.7.
12. Li, P., S. Banjade, H.-C. Cheng, S. Kim, B. Chen, L. Guo, M. Llaguno, J. V. Hollingsworth, D. S. King, S. F. Banani, P. S. Russo, Q.-X. Jiang, B. T. Nixon, and M. K. Rosen. 2012. Phase transitions in the assembly of multivalent signalling proteins. *Nature.* 483:336–340. https://doi.org/10.1038/nature10879.
13. Riback, J. A., L. Zhu, M. C. Ferrolino, M. Tolbert, D. M. Mitrea, D. W. Sanders, M.-T. Wei, R. W. Kriwacki, and C. P. Brangwynne. 2019. Composition dependent phase separation underlies directional flux through the nucleolus. Preprint at bioRxiv. https://doi.org/10.1101/809210.
14. Brangwynne, C. P., C. R. Eckmann, D. S. Courson, A. Rybarska, C. Hoege, J. Gharakhani…, 2009. Germline P granules are liquid droplets that localize by controlled dissolution/condensation. *Science.* 324:1729–1732. https://doi.org/10.1126/science.1172046.
15. Protter, D. S. W., B. S. Rao, B. Van Treeck, Y. Lin, L. Mizoue, M. K. Rosen…, 2018. Intrinsically disordered regions can contribute promiscuous interactions to RNP granule assembly. *Cell Rep.* 22:1401–1412. https://doi.org/10.1016/j.celrep.2018.01.036.
16. Martin, E. W., A. S. Holehouse, I. Peran, M. Farag, J. J. Incicco, A. Bremer…, 2020. Valence and patterning of aromatic residues determine the phase behavior of prion-like domains. *Science.* 367:694–699. https://doi.org/10.1126/science.aaw8653.
17. Brady, J. P., P. J. Farber, A. Sekhar, Y. H. Lin, R. Huang, A. Bah…, 2017. Structural and hydrodynamic properties of an intrinsically disordered region of a germ cell-specific protein on phase separation. *Proc. Natl. Acad. Sci. USA.* 114:E8194–E8203. https://doi.org/10.1073/pnas.1706197114.
18. Gomes, E., and J. Shorter. 2019. The molecular language of membraneless organelles. *J. Biol. Chem.* 294:7115–7127. https://doi.org/10.1074/jbc.TM118.001192.
19. Feric, M., N. Vaidya, T. S. Harmon, D. M. Mitrea, L. Zhu, T. M. Richardson…, 2016. Coexisting liquid phases underlie nucleolar subcompartments. *Cell.* 165:1686–1697. https://doi.org/10.1016/j.cell.2016.04.047.
20. Mitrea, D. M., and R. W. Kriwacki. 2016. Phase separation in biology; functional organization of a higher order. *Cell Commun. Signal.* 14:1. https://doi.org/10.1186/s12964-015-0125-7.
21. Yewdall, N. A., A. A. André, T. Lu, and E. Spruijt. 2021. Coacervates as models of membraneless organelles. *Curr. Opin. Colloid Interface Sci.* 52:101416. https://doi.org/10.1016/j.cocis.2020.101416.
22. Nott, T. J., T. D. Craggs, and A. J. Baldwin. 2016. Membraneless organelles can melt nucleic acid duplexes and act as biomolecular filters. *Nat. Chem.* 8:569–575. https://doi.org/10.1038/nchem.2519.
23. Wei, M.-T., S. Elbaum-Garfinkle, A. S. Holehouse, C. C.-H. Chen, M. Feric, C. B. Arnold, R. D. Priestley, R. V. Pappu, and C. P. Brangwynne. 2017. Phase behaviour of disordered proteins underlying low density and high permeability of liquid organelles. *Nat. Chem.* 9:1118–1125. https://doi.org/10.1038/nchem.2803.
24. Elbaum-Garfinkle, S., Y. Kim, K. Szczepaniak, C. C. H. Chen, C. R. Eckmann, S. Myong…, 2015. The disordered P granule protein LAF-1 drives phase separation into droplets with tunable viscosity and dynamics. *Proc. Natl. Acad. Sci. USA.* 112:7189–7194. https://doi.org/10.1073/pnas.1504822112.
25. Mitrea, D. M., J. A. Cika, C. S. Guy, D. Ban, P. R. Banerjee, C. B. Stanley…, 2016. Nucleophosmin integrates within the nucleolus via multimodal interactions with proteins displaying R-rich linear motifs and rRNA. *Elife.* 5:e13571. https://doi.org/10.7554/eLife.13571.
26. Brangwynne, C., P. Tompa, and R. Pappu. 2015. Polymer physics of intracellular phase transitions. *Nat. Phys.* 11:899–904. https://doi.org/10.1038/nphys3532.
27. Rivas, G., and A. P. Minton. 2018. Toward an understanding of biochemical equilibria within living cells. *Biophys. Rev.* 10:241–253. https://doi.org/10.1007/s12551-017-0347-6.
28. Horvath, I., R. Kumar, and P. Wittung-Stafshede. 2021. Macromolecular crowding modulates alpha-synuclein amyloid fiber growth. *Biophys. J.* 120:3374–3381. https://doi.org/10.1016/j.bpj.2021.06.032.
29. Ferrolino, M. C., D. M. Mitrea, J. R. Michael, and R. W. Kriwacki. 2018. Compositional adaptability in NPM1-SURF6 scaffolding networks enabled by dynamic switching of phase separation mechanisms. *Nat. Commun.* 9:5064. https://doi.org/10.1038/s41467-018-07530-1.
30. Mitrea, D. M., J. A. Cika, C. B. Stanley, A. Nourse, P. L. Onuchic, P. R. Banerjee…, 2018. Self-interaction of NPM1 modulates multiple mechanisms of liquid-liquid phase separation. *Nat. Commun.* 9:842. https://doi.org/10.1038/s41467-018-03255-3.
31. Yang, P., C. Mathieu, R. M. Kolaitis, P. Zhang, J. Messing, U. Yurtsever…, 2020. G3BP1 is a tunable switch that triggers phase separation to assemble stress granules. *Cell.* 181:325–345.e28. https://doi.org/10.1016/j.cell.2020.03.046.
32. Guillén-Boixet, J., A. Kopach, A. S. Holehouse, S. Wittmann, M. Jahnel, R. Schlüßler…, 2020. RNA-induced conformational switching and clustering of G3BP drive stress granule assembly by condensation. *Cell.* 181:346–361.e17. https://doi.org/10.1016/j.cell.2020.03.049.
33. Bouchard, J. J., J. H. Otero, D. C. Scott, E. Szulc, E. W. Martin, N. Sabri…, 2018. Cancer mutations of the tumor suppressor SPOP disrupt the formation of active, shase-separated compartments. *Mol. Cell.* 72:19–36.e8. https://doi.org/10.1016/j.molcel.2018.08.027.
34. Rayman, J. B., K. A. Karl, and E. R. Kandel. 2018. TIA-1 self-multimerization, phase separation, and recruitment into stress granules are dynamically regulated by Zn(2). *Cell Rep.* 22:59–71. https://doi.org/10.1016/j.celrep.2017.12.036.
35. Kojima, T., and S. Takayama. 2018. Membraneless compartmentalization facilitates enzymatic cascade reactions and reduces substrate inhibition. *ACS Appl. Mater. Interfaces.* 10:32782–32791. https://doi.org/10.1021/acsami.8b07573.
36. Crowe, C. D., and C. D. Keating. 2018. Liquid-liquid phase separation in artificial cells. *Interface Focus.* 8:20180032. https://doi.org/10.1098/rsfs.2018.0032.
37. Minton, A. P. 1981. Excluded volume as a determinant of macromolecular structure and reactivity. *Biopolymers.* 20:2093–2120. https://doi.org/10.1002/bip.1981.360201006.
38. Arakawa, T., and S. N. Timasheff. 1985. Mechanism of poly(ethylene glycol) interaction with proteins. *Biochemistry.* 24:6756–6762. https://doi.org/10.1021/bi00345a005.
39. Shkel, I. A., D. B. Knowles, and M. T. Record, Jr. 2015. Separating chemical and excluded volume interactions of polyethylene glycols with native proteins: Comparison with PEG effects on DNA helix formation. *Biopolymers.* 103:517–527. https://doi.org/10.1002/bip.22662.
40. Bekale, L., D. Agudelo, and H. A. Tajmir-Riahi. 2015. The role of polymer size and hydrophobic end-group in PEG-protein interaction. *Colloids Surf. B Biointerfaces.* 130:141–148. https://doi.org/10.1016/j.colsurfb.2015.03.045.
41. Wang, Y., and O. Annunziata. 2007. Comparison between protein-polyethylene glycol (PEG) interactions and the effect of PEG on

protein-protein interactions using the liquid-liquid phase transition. *J. Phys. Chem. B.* 111:1222–1230. https://doi.org/10.1021/jp065608u.

42. Qian, D., T. J. Welsh, N. A. Erkamp, S. Qamar, J. Nixon-Abell, G. Krainer, P. S. George-Hyslop, T. C. T. Michaels, and T. P. J. Knowles. 2022. Tie-lines reveal interactions driving heteromolecular condensate formation. Preprint at bioRxiv. https://doi.org/10.1101/2022.02.22.481401.
43. Ghosh, A., K. Mazarakos, and H. X. Zhou. 2019. Three archetypical classes of macromolecular regulators of protein liquid-liquid phase separation. *Proc. Natl. Acad. Sci. USA.* 116:19474–19483. https://doi.org/10.1073/pnas.1907849116.
44. Kaur, T., I. Alshareedah, W. Wang, J. Ngo, M. M. Moosa, and P. R. Banerjee. 2019. Molecular crowding tunes material states of ribonucleoprotein condensates. *Biomolecules.* 9:71. https://doi.org/10.3390/biom9020071.
45. Schuster, B. S., E. H. Reed, R. Parthasarathy, C. N. Jahnke, R. M. Caldwell, J. G. Bermudez…, 2018. Controllable protein phase separation and modular recruitment to form responsive membraneless organelles. *Nat. Commun.* 9:2985. https://doi.org/10.1038/s41467-018-05403-1.
46. Marianelli, A. M., B. M. Miller, and C. D. Keating. 2018. Impact of macromolecular crowding on RNA/spermine complex coacervation and oligonucleotide compartmentalization. *Soft Matter.* 14:368–378. https://doi.org/10.1039/c7sm02146a.
47. Yewdall, N. A., A. A. M. André, M. H. I. van Haren, F. H. T. Nelissen, A. Jonker, and E. Spruijt. 2022. ATP:Mg(2+) shapes material properties of protein-RNA condensates and their partitioning of clients. *Biophys. J.* 121:3962–3974. https://doi.org/10.1016/j.bpj.2022.08.025.
48. Proudnikov, D., and A. Mirzabekov. 1996. Chemical methods of DNA and RNA fluorescent labeling. *Nucleic Acids Res.* 24:4535–4542. https://doi.org/10.1093/nar/24.22.4535.
49. Reines, S. A., and C. R. Cantor. 1974. New fluorescent hydrazide reagents for the oxidized 3'-terminus of RNA. *Nucleic Acids Res.* 1:767–786. https://doi.org/10.1093/nar/1.6.767.
50. Taylor, N. O., M. T. Wei, H. A. Stone, and C. P. Brangwynne. 2019. Quantifying dynamics in phase-separated condensates using fluorescence recovery after photobleaching. *Biophys. J.* 117:1285–1300. https://doi.org/10.1016/j.bpj.2019.08.030.
51. Nakashima, K. K., A. A. M. André, and E. Spruijt. 2021. Enzymatic control over coacervation. *In* Methods in Enzymology. C. D. Keating, ed Academic Press, pp. 353–389. https://doi.org/10.1016/bs.mie.2020.06.007.
52. Bader, A. N., E. G. Hofman, J. Voortman, P. M. P. v. B. en Henegouwen, and H. C. Gerritsen. 2009. Homo-FRET imaging enables quantification of protein cluster sizes with subcellular resolution. *Biophys. J.* 97:2613–2622. https://doi.org/10.1016/j.bpj.2009.07.059.
53. Dong, X., A. Al-Jumaily, and I. C. Escobar. 2018. Investigation of the use of a bio-derived solvent for non-solvent-induced phase separation (NIPS) fabrication of polysulfone membranes. *Membranes.* 8:23. https://doi.org/10.3390/membranes8020023.
54. Dupuis, N. F., E. D. Holmstrom, and D. J. Nesbitt. 2014. Molecular-crowding effects on single-molecule RNA folding/unfolding thermodynamics and kinetics. *Proc. Natl. Acad. Sci. USA.* 111:8464–8469. https://doi.org/10.1073/pnas.1316039111.
55. Daher, M., J. R. Widom, W. Tay, and N. G. Walter. 2018. Soft interactions with model crowders and non-canonical interactions with cellular proteins stabilize RNA folding. *J. Mol. Biol.* 430:509–523. https://doi.org/10.1016/j.jmb.2017.10.030.
56. Groen, J., D. Foschepoth, E. te Brinke, A. J. Boersma, H. Imamura, G. Rivas…, 2015. Associative interactions in crowded solutions of biopolymers counteract depletion effects. *J. Am. Chem. Soc.* 137:13041–13048. https://doi.org/10.1021/jacs.5b07898.
57. Zwicker, D., and L. Laan. 2022. Evolved interactions stabilize many coexisting phases in multicomponent liquids. *Proc. Natl. Acad. Sci. USA.* 119. e2201250119. https://doi.org/10.1073/pnas.2201250119.
58. Currie, S. L., W. Xing, D. Muhlrad, C. J. Decker, R. Parker, and M. K. Rosen. 2022. Quantitative reconstitution of yeast RNA processing bodies. Preprint at bioRxiv. https://doi.org/10.1101/2022.08.13.503854.